Development and Testing of a Zero Stitch MLI Blanket using Plastic Pins for Space Use

Ryuta Hatakenaka[1], Takeshi Miyakita[2], Hiroyuki Sugita[3]
Japan Aerospace Exploration Agency, Tsukuba city, Ibaraki prefecture, 305-8505, Japan

Masanori Saitoh[4]
Orbital Engineering Inc., Yokohama city, Kanagawa prefecture, 221-0822, Japan

Tomoyuki Hirai[5]
Toska-Bano'k Co. Ltd., Bunkyo ward, Tokyo, 112-0014, Japan

New types of MLI blanket have been developed to achieve high thermal performance while maintaining production and assembly workability equivalent to the conventional type. Tag-pins, which are widely used in commercial applications to hook price tags to products, are used to fix the films in place and the pin material is changed to polyetheretherketone (PEEK) for use in space. Thermal performance is measured by using a boil-off calorimeter, in which a rectangular liquid nitrogen tank is used to evaluate the degradation at the bending corner and joint of the blanket. Zero-stitch- and multi-blanket-type MLIs show significantly improved thermal performance (ε_{eff} is smaller than 0.0050 at room temperature) despite having the same fastener interface as traditional blankets, while the venting design and number of tag-pins are confirmed as appropriate in a depressurization test.

Nomenclature

T_H = Temperature of the outermost layer of the MLI blanket on the hot side, K.
T_C = Temperature of the outermost layer of the MLI blanket on the cold side, K.
T_{shroud} = Temperature of the inner face of the aluminum shroud, K.
ε_{eff} = Effective emissivity of the MLI blanket, non-dimensional.
ΔQ_{MLI} = Increase in heat leak, W.
L_{stitch} = Length of stitch, mm.
q_{MLI} = Heat flux through the MLI blanket, W.
σ = Stefan-Boltzmann coefficient, W/(m²K^4).
A, B, C = Parameters of the equation to predict heat leak considering temperature dependence, non-dimensional.
P = Absolute nitrogen gas pressure in gas space [Pa]
V = Internal volume of gas space [m³]
n = Molecular number of nitrogen gas in gas space [mol]
R = Gas constant [(Pa m³)/mol K]
T = Temperature of nitrogen gas in gas space [K]
T_{sat} = Saturation temperature of nitrogen [K]
P_{sat} = Saturation pressure of nitrogen [Pa]
C_{tank} = Thermal mass of a nitrogen tank [J/K]
C_{LN2} = Thermal mass of liquid nitrogen in a tank [J/K]
L = Latent heat for vaporization of nitrogen [J/kg]
t = time [sec]
e_{fm} = Uncertainty of flow rate measurement due to the spec. of the flow meter [kg/s]

[1] Engineer, Thermal Systems Group, Aerospace Research and Development Directorate, hatakenaka.ryuta@jaxa.jp
[2] Engineer, Thermal Systems Group, Aerospace Research and Development Directorate, miyakita.takeshi@jaxa.jp
[3] Head, Thermal Systems Group, Aerospace Research and Development Directorate, sugita.hiroyuki@jaxa.jp
[4] Engineer, Engineering Group, saitoh@orbital-e.co.jp
[5] General Manager, Product Development Division, hirai0006@toska-banok.com

e_atm = Uncertainty of flow rate measurement due to atmospheric pressure variation [kg/s]

I. Introduction

The Multi-Layer Insulation (MLI) blanket, consisting of thin metallized polymeric films and spacer materials, has been widely used as a thermal control element on spacecraft. Thermal performance requirements, particularly for cryogenic astronomy satellites or exploration spacecrafts, have recently been increasing. Good thermal performance can be obtained by a relatively simple technique – more films and spacers, smaller layer density, fewer discontinuities, and so on. However, in case of MLI for spacecraft, the tolerance for a series of ground operations and the environmental conditions during ascent should also be considered. Since techniques to improve them - such as perforation holes, fasteners, sewing and taping of edges, and so on - tend to degrade the thermal performance of the blanket, whereupon it performs at far less than its potential[1].

This degradation is primarily attributable to the machine sewing[2][3], on all blanket edges and hook & loop fasteners. The stitches are used to fix the films and spacers, and reinforce the edges. To substitute the former, tag-pins, widely used in commercial applications to hook price tags to products, seem suitable because they can fix layers without compressing them. Hook and loop fasteners are attached to the innermost layer with adhesives as a substitute for sewing. This blanket design is called as a zero-stitch MLI in this paper. A beneficial feature of zero-stitch MLI using tag-pin is the ease of blanket production and handling; a tag-pin can be easily planted into a blanket by using a commercial planting tool (tag-gun) as-is, while the worker can handle the stacks of films and spacers as a blanket when the pitch of pins are properly designed. In addition, another type of blanket, called as multi-blanket, staggered lapped MLI in this paper, which facilitates the workability of blanket connections far more than zero-stitch MLI, is also presented as a promising option.

The MLI thermal performance is measured with various types of apparatus in literature[4]-[9]. A boil-off calorimeter, which facilitates temperature uniformity, is one of the most famous methods. In particular, the vertical-cylinder-type boil-off calorimeter has the advantage whereby gravity does not apply in the direction to press the layers. In this paper, a unique rectangular boil-off calorimeter is used to simulate a satellite body and amplify the degree of performance degradation. In addition, a method to correct a shift of flow rate driven by tiny atmospheric pressure variation is presented. In case of high performance MLI, the amount of this effect becomes equivalent to the flow rate level and cannot be cancelled by simple averaging procedure.

The targeted thermal performance is 0.040W/m^2 at a temperature range of T_H=80K, Tc=120K, which is the current mission requirement of the SPICA next-generation infrared space telescope [10]. Since it was difficult to perform the test within this temperature range in our facility, a heat leak through MLI in the range is predicted considering temperature dependency, where the equation form is fixed based on literature and coefficients are determined using three points of test data at different temperature levels.
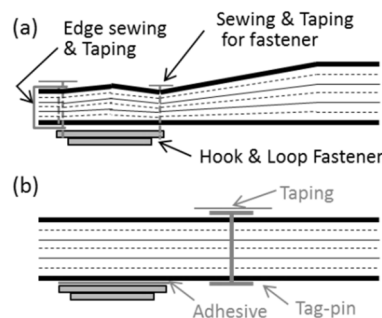

Fig. 1 Schematic of (a) traditional and (b) zero-stitch blanket

II. Materials and Method

A. Tag-pin made of PEEK

Most commercial tag-pins are made of nylon, the outgas property of which is incompatible with the general outgas criteria for spacecraft, while no other products are made of materials suitable for space use. Accordingly, with the latter in mind, a tag-pin made of polyetheretherketone (PEEK) was newly developed (Fig. 2). The material is chosen by considering fluidity during injection molding, flexibility during planting into a target, and tolerance for temperature and space environment. A tag-gun (Toska-Bano'k, 303Z, unchanged from the commercial product, Fig. 3) is used to plant the tag-pin into a target, while the length and diameter of the filament of this tag-pin are 15 and 0.3mm respectively. The head thickness on one side is as flat as 0.3mm, which facilitates covering the head by taping the outermost layer of the blanket. Prior to the blanket design, a

series of tensile tests on tag-pins made of PEEK were performed (Fig. 4). There are two types of fracture - one involves slipping through the hole by bending the flat head, and the other is a tensile fracture at the root of the filament itself. When the hole diameter is equal to that of the needle of the planting device, the former occurs at 18.6 +/-2.7N (10 samples were tested), but it is far more prone to occur when the hole expands. By taping the flat head tightly (Fig. 3, right-hand side), the former can be avoided, whereupon the latter occurs at 18.6 +/-0.8 N (20 samples were tested). The blanket design is performed based on this value.
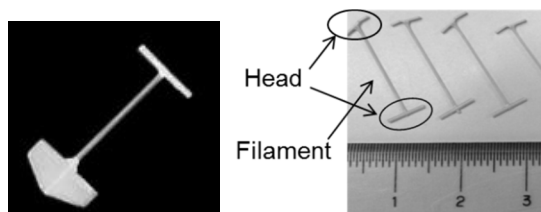
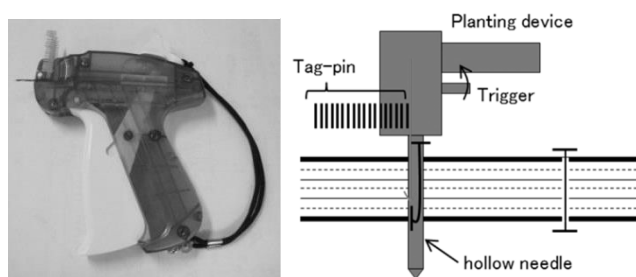Fig. 2 Commercial tag-pin (left) and newly developed tag-pin (right)

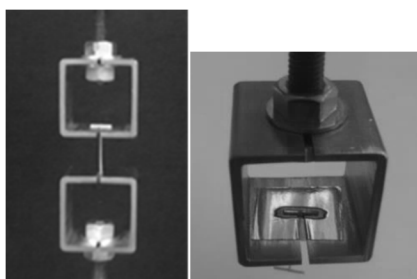Fig. 3 Planting device and tag-pin planting method

Fig. 4 Tensile strength test method

B. Design of Zero-stitch MLI and Multi-blanket, staggered lapped MLI

Two types of new MLI blanket using tag-pin are designed; zero-stitch MLI blanket and multi-blanket, staggered lapped MLI. Table 1 shows a comparison between these two, the details of which are explained as follows. The blanket design is intended to be realistic as a blanket for space use in terms of toughness, venting design, workability and so on, since the thermal performance is significantly affected; not only by the layer stacks, but also by the detailed design.

(1) Zero-stitch MLI blanket

The zero-stitch MLI blanket is a new type of MLI blanket in which films and spacers are fixed together using a tag-pin. Hook & loop fastener (A8693Y-71/B2790Y-00, 16mm side, Kuraray Fastening Co., Ltd.) attached to the innermost layers without machine-sewing, is used to fix the blanket in place to the spacecraft body.

The so-called "fastener patch technique" described in this paper has already been used for a Japanese spacecraft "Kounotori (HTV)" to improve MLI thermal performance. Table 1 shows a picture and schematic illustration of this technique. The hook & loop fastener are firstly sewn to a fiber-reinforced polyimide film by machine-sewing, and then attached to the innermost layer of the mother-blanket using double-faced adhesive and thermal control tape. This technique provides adequate strength to withstand the "attach and detach" procedure of the blanket. Note that the fastener is attached directly to the innermost layer only via both-faced adhesives (Y966, 3M) in this paper to reduce the cost of the test pieces since this difference does not affect the thermal performance data.

The lack of any stitch renders the blanket softer and more fragile (more easily torn) compared to traditional MLI blankets. To improve this point, one extra-thick and strong sheet (0.2mm-thick polyethylene terephthalate (PET) in our test) was added as the innermost layer, to facilitate handling of the blanket when attached or

3

detached by a worker, by holding this thick layer. Basically, the blanket edges are not sewn either since they are connected by the inter-leaved lapping method. To simplify the blanket design, films and spacers have the same length, despite differing perimeter lengths at the corner, since the lapping length need not be uniform. In practical usage, there should be some free edges, which should be treated with some other techniques. Such detailed design is closely linked to the specific spacecraft configuration and is thus not discussed in this paper.

For actual applications, the design of the layer stacks should be optimized considering mass, cost, thermal requirement, temperature range, and so on. In our experiment, the number of layers is set at 24 for comparison to the other blankets, while the number of nets is doubled in each layer. Inai reported that conductive thermal resistance inside the spacer material was three orders smaller than contact thermal resistance in the case of the glass fiber spacer [11]. Accordingly, the conductive thermal resistance between films is expected to double by doubling the spacer, since the number of contact points increases from two to four. Another advantage of the double net system is that it does not significantly influence the venting design, unlike the increase in films, which hinders the same. The distribution of nets can be biased toward the cold side in terms of optimization, since heat conduction is more dominant than radiation at a lower temperature. However, the effect of the biased distribution of net is limited (or negligible in cryogenic application), meaning the nets are equally distributed in this paper to avoid increasing the experimental parameters.
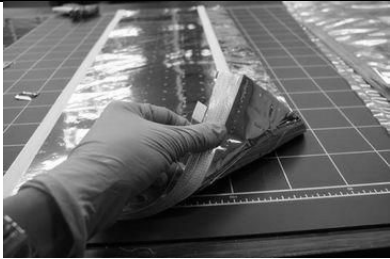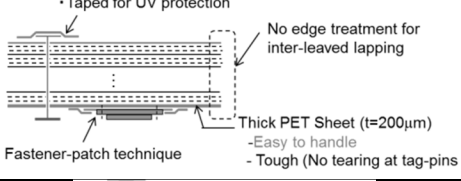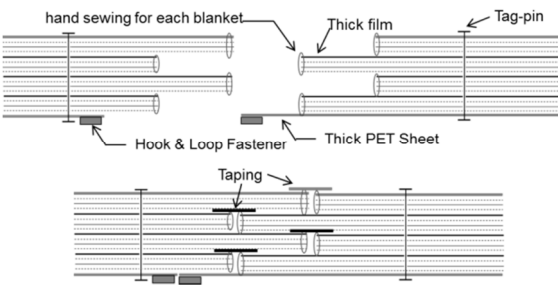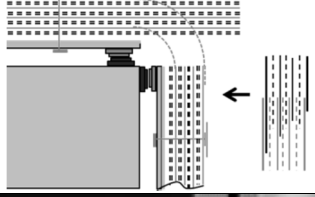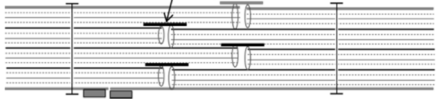
The number of tag-pins is definitely a crucial thermal performance parameter, since they establish a direct conductive heat path from hot to cold sides without any contact resistance. Their number and placement are to be designed in terms of handling and strength against ballooning under depressurization. The criterion of differential pressure between the inside and outside of th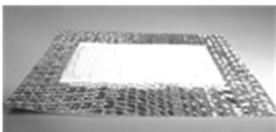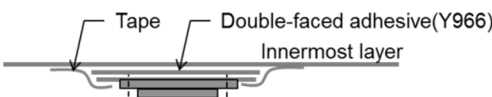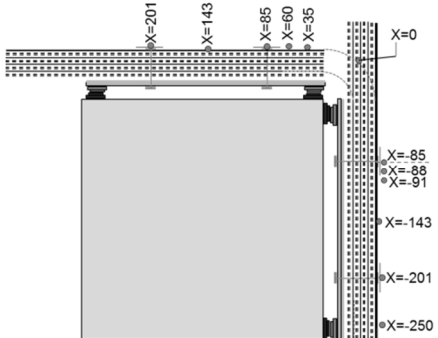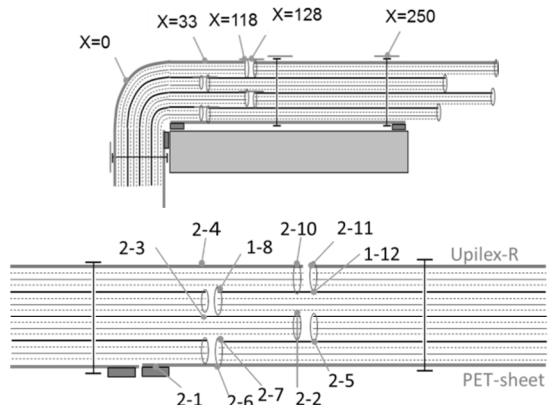e blanket is set at 100Pa. By considering the tensile strength of the pin and safety factor (set at 5.0), the minimum number of pins is calculated as 25 per square meter. However, the pitch of tag-pins is actually set at approximately 110×110mm (64 per square meter), considering ease of handling, while it is difficult to discuss this point quantitatively. The pins are uniformly placed to avoid load concentrations on specific pins due to ballooning, while the blankets are connected via inter-leaved lapping, meaning pins are not planted near the edges as illustrated in Table 1. The perforation specification is set at Φ2.0mm, 25×25mm pitch, random pattern and a depressurization test (Sec. C) confirms that the maximum differential pressure is lower than the criterion.

(2) Multi-blanket, staggered lapped MLI

The blanket connection is known to be one of the major reasons for performance degradation, while the inter-leaved lapping method, in which films and spacers are fixed with tape one by one, is the optimal choice to minimize heat loss. Although the zero-stitch MLI blanket is designed to be connected by this method, it is a relatively delicate operation and thin inner films (6μm thick) are frequently torn off when the connection tape is detached. Worse still, a blanket connection should be performed on-site in the spacecraft assembly process. Adopting this further extends the required spacecraft assembly, and raises the risk of a schedule delay due to unexpected fracture of the films.

The second idea, which is called as a multi-blanket, staggered lapped MLI in this paper, is designed to overcome this problem. A snapshot and schematic image are shown in Table 1. A (mother-) blanket is divided into four sub-blankets, the edges of which are hand-sewn. Each sub-blanket is connected to a neighboring sub-blanket by a butting-joint with taping, and the connection locations are staggered in each sub-blanket. Four sub-blankets and a thick PET sheet (t=200μm) are fastened into one (mother-) blanket using tag-pins made of PEEK. The number of tag-pins and perforation specification are equal to those for the zero-stitch blanket since the layer stack is the same. Adopting this type considerably improves the workability of the blanket connection; only 4 times are needed for this type, while 64 times (24 films and 48 nets) are needed for the zero-stitch blanket. In addition, it enables us to attach & detach repeatedly using relatively thick film (25μm) for the outermost layer of each sub-blanket. Another merit of this type is the uniformity of MLI thickness. Either the thickness of MLI or the layer density should be doubled in case of inter-leaved lapping (Fig. 13), while they remain basically unchanged in the case of the butt joint. The uniformity of thickness facilitates configuration control for the worker. In addition, this type is considered easy to adopt in actual spacecraft projects with little resistance since each sub-blanket is manufactured using a production line in a normal MLI manufacturer. Note that the edges of sub-blankets are sewn loosely by hand in this paper, while a test piece whose sub-blankets are machine-sewn is to be tested in future.

4

Table 1 Comparison between zero-stitch MLI and Multi-blanket, staggered lapped MLI

	Zero-stitch MLI blanket	Multi-blanket, staggered lapped MLI
Snapshot		
Structure		
Blanket Connection		
Thickness		
Fastener		
Perforation	$\Phi2.0$mm, pitch=25×25mm, random pattern (The validity is examined in Sec. C.)	
Location of T/C		

5

(3) Depressurization Test

The number of layers, perforation hole specification, fastener, and fixation method (machine sewing or tag-pin) should be discussed, not only from a thermal performance perspective, but also with practical utilities such as handling, outgas, cost, vibration conditions and depressurization environment during the ascent in mind. Concerning compliance with the depressurization environment during launch, sufficient knowledge exists of the appropriate perforation specifications for traditional 12-layer MLI blankets [12], but there is no information on zero-stitch MLI blankets. Accordingly, a depressurization test is performed to confirm compliance with environmental conditions prior to the thermal performance test.

Figure 5 shows a schematic of the depressurization facility, with details of the test setup and procedure introduced in the previous paper [12]. The pressure profile is controlled by the open-looped voltage control of an electric valve. Pressure in the chamber ($P_{chamber}$) is measured using two types of sensors: a strain gauge type (PAB-A-200KP) for full range measurement and temperature control "Baratron" (capacitance manometer, 627D21TQC2B) for lower pressure levels (< 2.6 kPa). Differential pressure between the inside and outside of MLI is measured with plastic tubes inserted between the layers and connected to differential pressure sensors (PT-103B-A, 1000Pa F.S.). Figure 5 shows the reference ports of differential pressure as set inside the chamber. The inflation height (z) is measured using a laser displacement meter (LK-G400).

To simulate the worst case in terms of venting, the test was performed with the following configuration (Fig. 6):

1) All blanket edges were sewn with a sewing machine and covered with tape
2) The blanket was fixed to a flat plate with tape
3) The innermost thick PET sheet had no perforation hole

The transient behavior of a zero-stitch MLI under a depressurization environment is shown in Fig. 7, while a snapshot of the MLI surface around a tag-pin at an inflation peak is shown in Fig. 8. The general trend – whereby inflation and differential pressure peak at relatively low pressure levels - is equivalent to that of traditional MLI as reported in the previous paper [12]. Tag-pins suppress inflation of the blanket and are tensed with a tensile force proportional to the differential pressure between the inside and outside of the blanket. The peak MLI thickness value (approximately 40mm) exceeds the length of the tag-pins (15mm), since the innermost layer (thick PET sheet) was floated from the flat-plate jig. The peak value of differential pressure is approximately 90Pa, which is below the design criteria of 100Pa, and no damage was seen in the blanket and tag-pins after ten times depressurization. Based on this test, the zero-stitch MLI blanket design is confirmed to meet the requirement against the depressurization environment during launch.
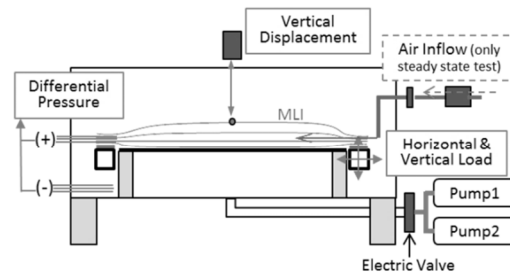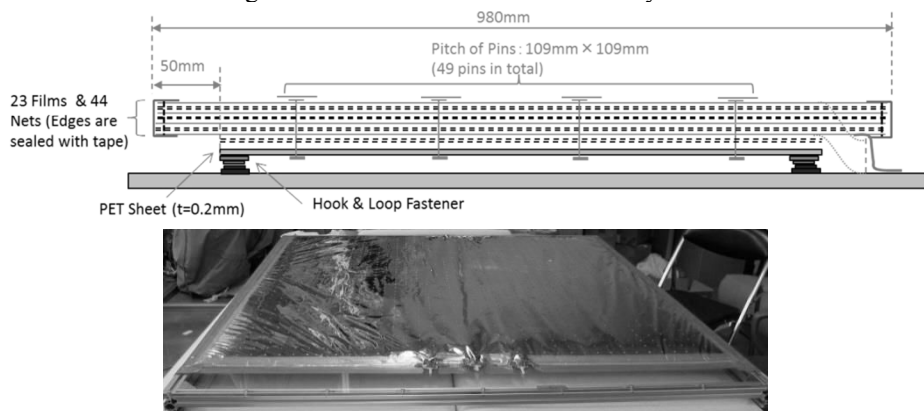

Fig. 5 Schematic of the measurement system

Fig. 6 Test configuration to simulate the worst case (upper: schematics, lower: a snapshot)
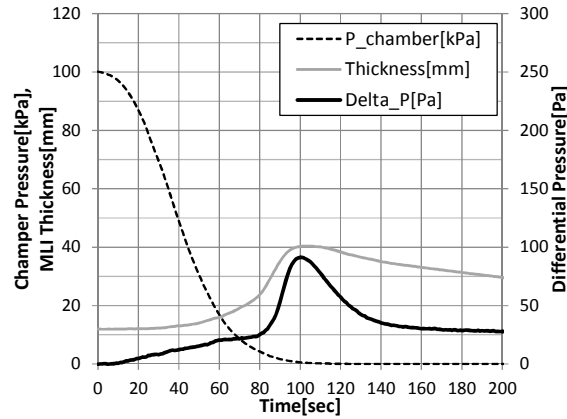
This document is provided by JAXA.

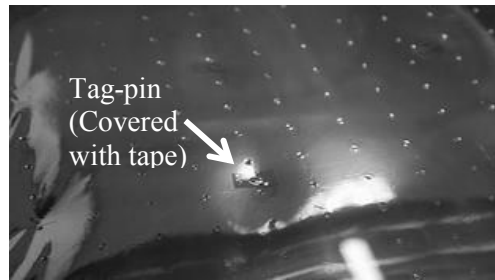Fig. 7 Historical trend during the depressurization

Fig. 8 Snapshot of the MLI surface around a tag-pin at peak

C. Thermal Performance Test
C.1 Setup for the Thermal Performance Test

The thermal performance of the MLI blanket is evaluated using the boil-off calorimeter method involving liquid nitrogen; the setup for which is shown in Fig. 9. The measurement tank is located between two guard tanks and a test piece (MLI blanket) is attached around the three tanks collectively. This configuration enables uniform temperature distribution around the measurement tank along the axial direction. A temperature-controlled aluminum shroud surrounds the test piece, where the temperature distribution in the inner surface of the shroud is within 1.0°C.

To evaluate the degree of degradation due to the corner and attachment method, two types of liquid nitrogen tank are used: one is a traditional cylindrical tank, and the other a rectangular tank, which simulates a spacecraft body. The surface area of the measurement tank is the same for both types. A hook & loop fastener is attached to the edges of the rectangular tanks using adhesive tape when the test piece has a hook & loop interface. Since the fastener is attached over the entire length, as illustrated in Fig. 10, uniform temperature distribution in an axial direction - the main advantage of this method - is maintained.

Another feature of our experimental setup is surface finishes. The outermost and innermost layer of the MLI blanket, the inner surface of the shroud, and the outer-surface of the liquid nitrogen tanks are all high-emissivity surfaces, as listed in Table 2. This design aims to minimize radiative thermal resistances between MLI surfaces to the shroud or tank and minimize the effect of uncertainty of contact heat transfer between the innermost surface of MLI and the tank surface.

The flow rate of nitrogen gas flow evaporated from the measurement tank is measured using three types of the flow meter as follows:
  (a) Wet-type volume flow meter W-NK-0.5 (Shinagawa Corp.)
  (b) Mass flow meter CMS-9500 (Azbil Corp.)
  (c) Soap-film volume flow meter (50ml type, time measured manually, for cross-checking)
The wet-type flow meter allows us to measure a wide-ranging flow rate (from 0.016 to 5000mL) with a single flow meter, but has the disadvantage of yielding fluctuating flow rate due to the difficulty in rotating the measurement wheel when the flow rate is small, while the averaged flow rate calculated from the integrated flow rate is considered reliable owing to its measurement principle. Conversely, the mass flow meter is suitable for this experiment since the final desired value is not a volume flow rate but a mass flow rate, despite the relatively narrow measurement range. In this paper, some of the data is taken with (a) and the remainder with (b). Another experiment confirmed that the averaged flow rates of these two flow meters match.

The temperatures of the tanks and MLI surface are measured using a Type-T thermocouple, and the places are individually chosen per test piece. The diameter of the copper and constantan wire is 100μm, while the wires of the thermocouple for the MLI surface are routed on the surface for a certain length and taped to equal to a

7

thermal anchor. The tip of the thermocouple is electrically insulated with Kapton tape, and covered with a piece of vapor-deposited polyimide tape (UTC-025R-NANA, Ube Industries, Ltd.) to form the same surface as MLI. By checking for any drop in MLI surface temperature, the source of a heat leak can be detected (Fig. 11). The relationship between surface temperature and heat flux calculated with the emissivity values (0.9 for the shroud, 0.7 for the MLI surface) and T_{shroud} (=300K) is also shown in Fig. 11.
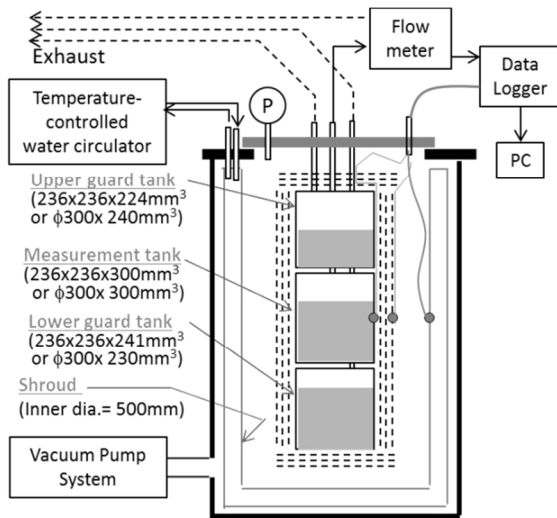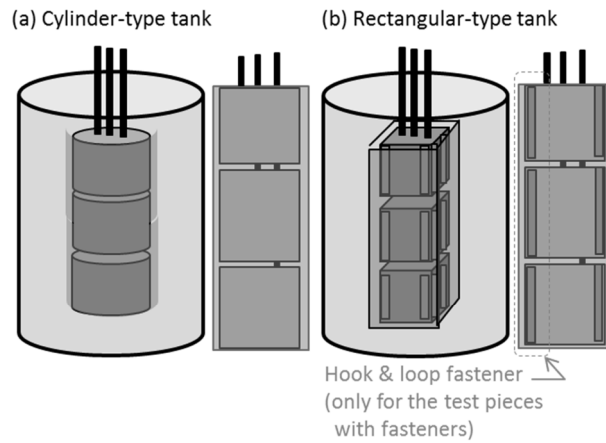

Fig. 9 Schematic image of the experimental setup

Fig. 10 Cylinder and Rectangular tank

Table 2 List of surface finishes

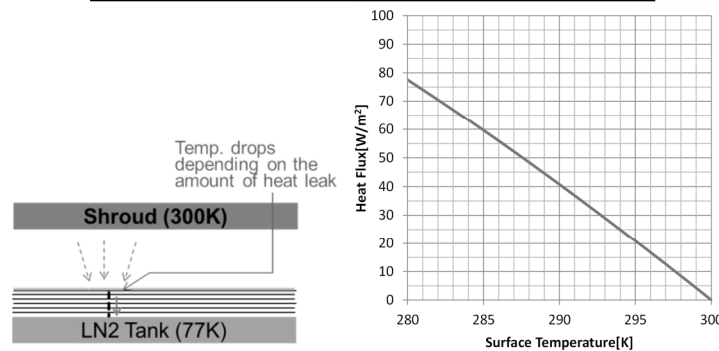| Place	Surface finish
Outerside of MLI	Polyimide surface(25μm thick)
Innerside of MLI	Polyimide surface(25μm thick) or PET surface (200μm thick)
Innerside of Shroud Outerside of Tanks	Black anodize aluminum

Fig. 11 Relationship between surface temperature drop and heat flux

C.2 Data Correction method for atmospheric pressure variation
C.2.1 Overview

Figure 12 shows an example of the variation in flow rate observed in the boil-off calorimetric test. This data is not the result of our new blanket, but the one we presented in a previous study [13]. "MFM1" is a flow rate from the center tank (measurement tank), while "MFM2" is that from the lower guard tank, both of which are measured with the flow meter (b) in Sec. C.1. As seen in the last half of the graph, the value of the flow rate varies, even though the shroud temperature is maintained at a constant value. The atmospheric pressure variation, which is taken by the Japan Meteorological Agency at a distance of 1 kilometer from the test site, is also shown in the same graph and the variation in flow rate seems synchronized to the atmospheric pressure variation.

Even though the flow meter outlets are open to the atmosphere, the pressure level itself does not affect the measurement result, since mass flow meters are used. In addition, the variation peaks at only 2% of the pressure level, even when the weather condition changes dramatically. Conversely, the variation in flow rate peaks at 100% of the nominal flow rate when the flow rate is as small as few tens of milliliters per minute. From these facts, there should be a mechanism in which a differential, rather than absolute value, of atmospheric pressure affects the flow rate.
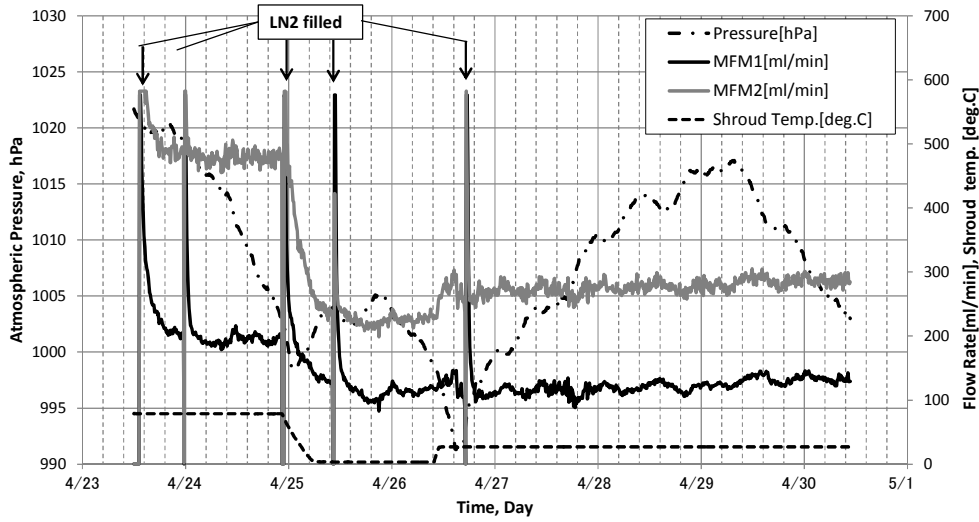
8

Fig. 12 Flow rate variation and atmospheric pressure variation

B.2.2 Effect of atmospheric pressure differential on flow rate measurement

There are two possible mechanisms explaining how the differential of atmospheric pressure affects the flow rate as follows:

(1) Expansion and Shrinkage of gas in the gas space

The nitrogen gas enclosed in the gas space between the boil-off tank and the flow meter outlet expands or shrinks due to a change in outlet pressure of the flow meter, which leads to a variation in flow rate. The amount of flow rate variation attributable to this effect can be calculated with an equation of state for perfect gas. By assuming that uniform gas temperature, regardless of atmospheric pressure, and assuming a constant internal gas space volume (V), the following equation can be obtained as temporary differentials of equation of state for perfect gas:

$$\frac{dP}{dt} \cdot V = \frac{dn}{dt} RT , \qquad (1)$$

where P denotes the nitrogen gas pressure in the gas space, n denotes the molar number, R is the gas constant, and T denotes the absolute temperature. Subsequently, the mass flow rate due to pressure variation can be calculated as follows:

$$\frac{dn}{dt} = \frac{dP}{dt} \cdot \frac{V}{RT} \qquad (2)$$

For our test setup, V is approximately 1.1×10^{-2} m³. When we assume $T= 298$K (room temperature) and dP/dt =0.020Pa/sec (typical value of atmospheric pressure variation), the variation in mass flow rate (dn/dt) is approximately 8.8×10^{-8} mol/sec, which is equivalent to 0.13 ml/min when it is 1 atm. and 25 deg. C. This is negligible compared to the flow-rate level, which is in the order of a few tens of ml/min at minimum.

(2) Shift in the two-phase equilibrium point

When the atmospheric pressure varies, the two-phase equilibrium point of nitrogen in the measurement tank shifts, whereupon the saturation temperature (T_{sat}) also changes. The evaporation rate of nitrogen will change transiently until the whole system reaches a new equilibrium point. Jacob et al. [14] introduced this phenomenon, and a specially designed, diaphragm-type pressure controller is used in their paper. Since no detailed information is included in the paper, we performed a quantitative calculation as follows:

The change in equilibrium temperature based on the pressure change (dT_{sat}/dP_{sat}) is only 8.4×10^{-5} K/Pa, meaning the time derivative of equilibrium temperature (dT_{sat}/dt) driven by the atmospheric pressure variation can be calculated as 1.7×10^{-6} K/sec using the following equation when assuming $dP/dt = 0.020$Pa/sec.

$$\frac{dT_{sat}}{dt} = \frac{dP}{dt} \cdot \frac{dT_{sat}}{dP_{sat}} \qquad (3)$$

Although this value seems tiny, it should also be noted that the amount of heat leaking through MLI is also tiny (approximately 0.1W at minimum) to change the temperature of the tank and liquid nitrogen inside, the thermal mass of which is considerable. The thermal mass of the measurement tank (denoted as C_{tank}) can be calculated from the dimensions as approximately 3500J/K, while that of liquid nitrogen (denoted as C_{LN2}) is approximately 17500 J/K when the tank is half-filled. The relationship between the change in mass flow rate ($\Delta dm/dt$) and the time derivative of the equilibrium temperature is written as:

9

$$\Delta \frac{dm}{dt} = \frac{dT_{sat}}{dt} \cdot \frac{C_{\tan k} + C_{LN2}}{L},$$ (4)

where L denotes the latent heat of nitrogen. When we assume $dP/dt = 0.020$Pa/sec and the tank is half-filled with liquid nitrogen, $\Delta dm/dt$ can be calculated as 1.81×10^{-7}kg/sec, which corresponds to 9.6ml/min at 1atm, 25deg. C. This value is equivalent to the flow rate value in case of high performance MLIs.

The last half of the graph shown in Fig. 12 is suitable for checking this idea, since the shroud temperature is maintained at 3 deg. C for as long as four days without filling liquid nitrogen during this period. The data from 12 o'clock 27th, when the system has already reached an equilibrium, to the end of the graph is used. The liquid nitrogen is not considered to have dried up in any of the three tanks in this period according to the temperature trend measured on the tank surfaces.

Figure 13 shows a comparison between the actual data and the calculation result based on Eq. (4), where the raw data and data smoothed by moving-averaging for +/-30mins are shown. Atmospheric pressure is measured every 10mins, during which time the typical pressure change is approximately 0.1-0.2hPa, which is very close to the resolution limit (0.1hPa) of the pressure sensor and explains the data dispersion seen in the upper graph. Conversely, when the data is moving-averaged for +/-30mins, the pressure change is multiplied by 6, falls in the measurement resolution and the curve is smoothed as seen in the bottom graph. The actual variation in flow rate is a subtraction between the flow rate at the time (not averaged, just sampled) and the average flow rate for the whole period (about 4 days). The fluctuation in flow rate variation is not close to the resolution limit of the flow meter and is thus considered attributable to other factors (e.g. electrical noise, local pressure variation around the test facility, and so on). The curves of the flow rate variation are also smoothed in the bottom graph of Fig. 13 by moving-averaging for +/-30mins (7data used), while it can be further refined using all data taken in every 1sec in our test.

The historical trends of these three curves in the bottom graph correlate well, which indicates the validity of this estimation method. It should be noted that the absolute value of variation is proportional to the total thermal mass, which is mostly determined by the amount of liquid nitrogen in the tank. In this paper, since the level of liquid nitrogen cannot be measured in our facility, it is assumed that all tanks are half-filled. Accordingly, the quantitative agreement seen in Fig. 13 is coincidental.
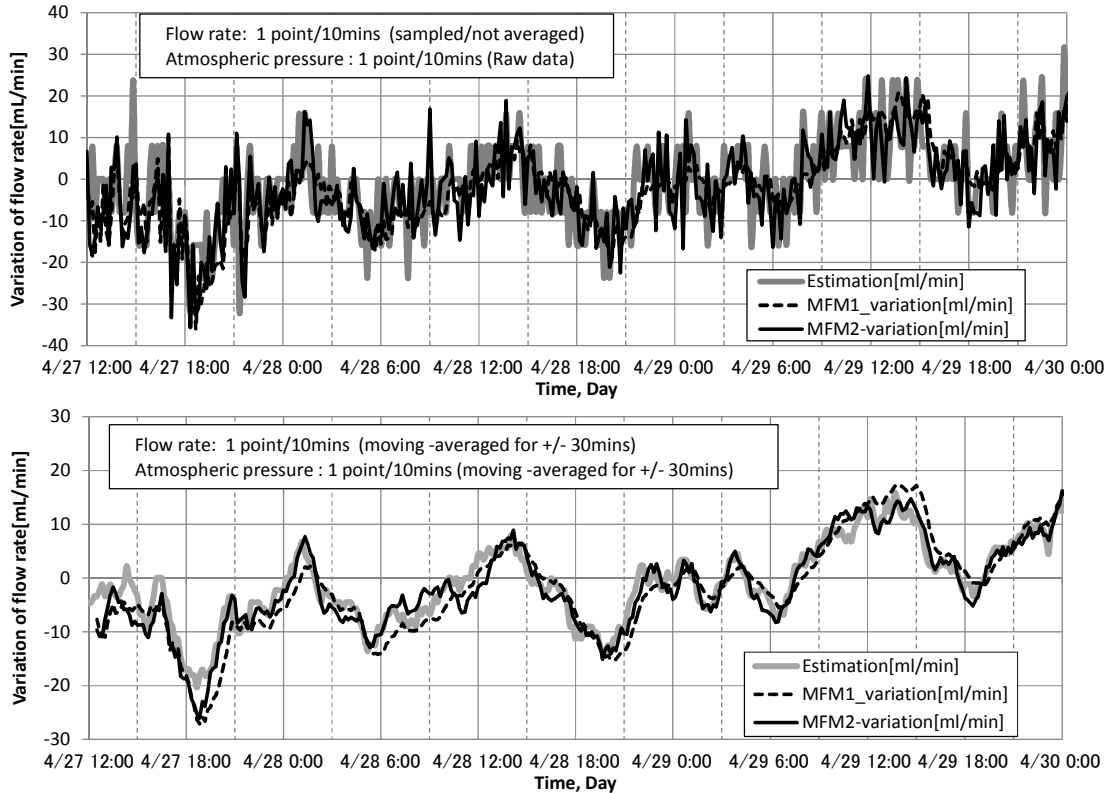
Fig. 13 Comparison between the actual variations of flow rate and the estimation result
(Upper: Raw data(sampled 1 point/10mins, Bottom: smoothed by moving-averaging)

B.2.3 Data correction method and the width of error bars

The atmospheric pressure variation is a long period, the cycle of which may extend beyond a few days, while the equilibrium data is usually taken for only 1-2 hours with the time constraint in mind. Accordingly, the

10

shift in the flow rate due to the atmospheric pressure variation cannot be eliminated by time-averaging; the heat leak will be underestimated with increasing pressure and vice versa, even after time-averaging is performed for a few hours. In this paper, to obtain the center value of each plot, a moving-averaged flow rate for +/-30mins is calculated and then corrected based on Eq. (4) using a moving-averaged atmospheric pressure variation and assuming the liquid nitrogen is half-filled.

In addition, error bars are drawn considering the uncertainty of the liquid nitrogen level. Since the level is not measured in our test, the uncertainty of the thermal mass $e(C_{LN2})$ is +/- 17500 J/K (from empty to full). The uncertainty of the amount of data correction is calculated as follows:

$$e\left(\Delta\frac{dm}{dt}\right) \approx \frac{dP}{dt} \cdot \frac{dT_{sat}}{dP_{sat}} \cdot e(C_{LN2}) = 1.47 \times \frac{dP}{dt} \qquad (5)$$

As Eq. (5) indicates, the uncertainty depends on the weather condition during the test period. The total uncertainty of the flow rate, which is used to determine the width of the error bar for each plot, is calculated as follows:

$$e_{total} = \sqrt{(e_{fm})^2 + e\left(\Delta\frac{dm}{dt}\right)^2} \qquad (6)$$

where e_{fm} denotes the measurement uncertainty of the flow meter.

B.3. Test Cases

A list of test cases for thermal performance is shown in Tables 3. Basically the materials listed on Table 4 are used in common among all test pieces unless otherwise specified. There are three types of connection method in this paper, which are shown in Fig. 14.

Concerning Nos. 1-3, MLI is installed to the boil-off tank using a "one-by-one method" to simulate a near-ideal configuration, in which the lapping width of inter-leaved lapping is approximately 30-50mm. The same test piece (MLI) is used for both Nos. 1 and 2 to evaluate performance degradation at bending corners.

Nos. 4 and 5 are traditional MLI blankets, each of comprising four small blankets installed into each face of the rectangular tank. The edges are machine-sewn and taped (see Fig. 1 (a) for detail) for all circumferences, and hook & loop fasteners (A8693Y-71/B2790Y-00, 16mm side, Kuraray Fastening Co., Ltd.) are attached at the two longer sides (see Fig. 10 for fastener location) via machine-sewing.

No. 6 is another simple idea called the "MLI-patch technique" in this paper. Its concept is quite simple; just hide stitches of traditional MLI blankets using another traditional blanket, as shown in Fig. 15. The key parameter is lapping length; the distance between the stitch of the base MLI and that of the patch MLI. Since local thermal performance in the region where the distance from the edge is less than 50mm declines according to our previous paper[8], it is considered that the lapping length should be larger than 100mm in case that the edge of the MLI patch is also sewn. In this paper, however, it is set at approximately 65mm, since patch-MLI may cover almost all the surface (tank width = 237mm) of base MLI when it is 100mm.

Nos. 7 and 8 are the new types of MLI blanket explained in Sec. IIB. It should be noted that the perforation specification differs from Nos. 1 to 6.

No. 9 is another type of MLI called a Non-Interlayer-Contact-Spacer MLI, the result of which is presented for details in the other paper [15]. In this paper, the plot of this MLI is also drawn in graphs for readers' convenience.

Table 3 List of test cases

No.	Name	Layers	Connection	Perforation	Tank
1	Reference MLI(1)	Film x12/Net x11	Inter-laeved lapping x1		Cylinder
2	Reference MLI(2)	Film x12/Net x11	Inter-laeved lapping x1		Rectangular
3	Reference MLI(3)	Film x24/Net x23	Inter-laeved lapping x1	Dia.=2mm, 50mmX50mm, random	
4	Traditional_MLI(1)	Film x12/Net x11	Butting joint x4		
5	Traditional_MLI(2)	Film x12/Net x11	Simple overlap x4		
6	Traditional+MLI Patch	Film x12/Net x11	Butting joint x4		
7	Zero_stitch_MLI	Film x24/Net x46	Inter-laeved lapping x4	Dia.=2mm, 25mmX25mm, random	
8	Multi-blanket, staggered lapped	Film x24/Net x46	Staggered lapping x4		
9	Non Interlayer Contact Spacer MLI	Film x 6	Inter-laeved lapping x4	N/A	

11

Table 4 Material List for test pieces

| Outermost film	Vapor-deposited polyimide film (UTC-025R-NANN, Ube Industries, Ltd., 25μm thick). The polyimide face is directed to the external.
Inner reflective films	Vapor-deposited polyimide film (KF-6B, Kaneka Corp. 6μm thick)
Spacer	Net spacer (KN-20, Kaneka Corp.)
Innermost film	Vapor-deposited polyimide film (UTC-025R-NANN, Ube Industries, Ltd., 25μm thick). The polyimide face is directed to the external
Connection tape	Either of UTC-025R-NANA (Ube Industries, Ltd.) or UTC-025R-ANNA (Ube Industries, Ltd.) is chosen to make the same surface optical property as the surroundings.
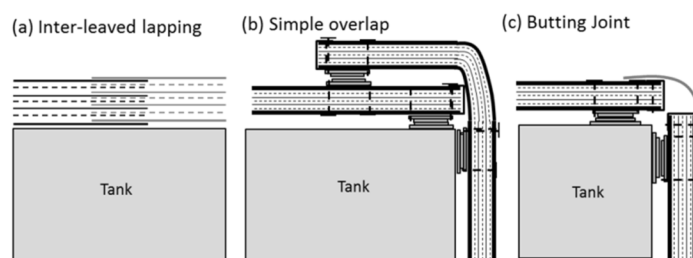
Fig. 14 Connection Method
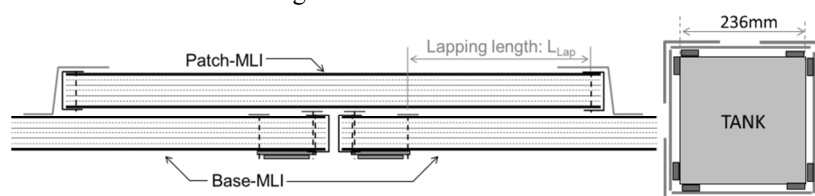
Fig. 15 Schematic image of MLI patch technique

III.   Results and Discussion

The heat fluxes, calculated from the flow rates of evaporated nitrogen gas from the measurement tank and with the shift corrected due to variation in atmospheric pressure, are shown in Fig. 16. Details of the test results and discussion will be given in the following sections.
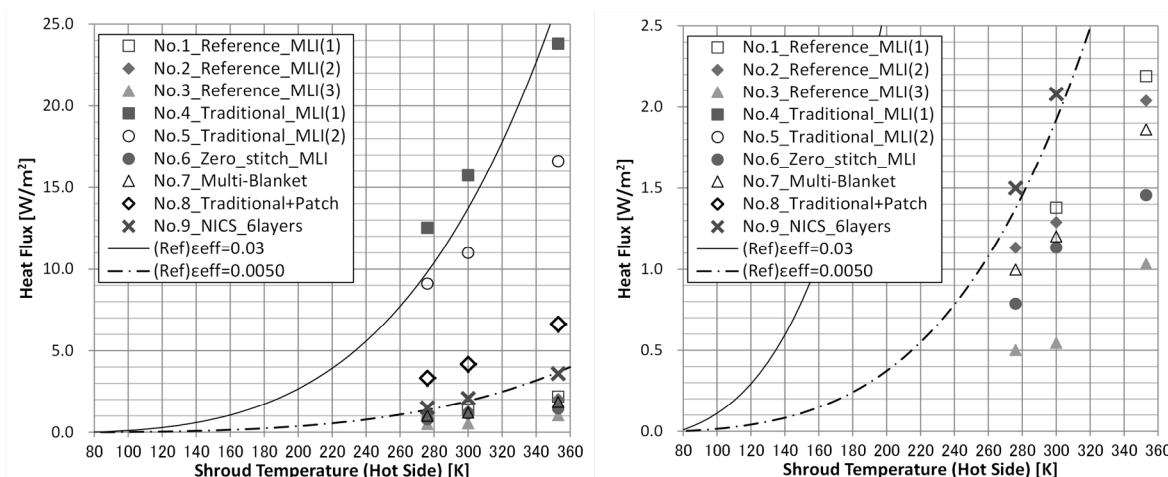

Fig. 16 Relationship between shroud temperature and heat flux (Upper: full range, lower: enlarged)

A. Reference MLIs (Nos. 1-3)

It is quite important to control and measure the layer density of the MLI blanket, since it significantly affects thermal performance. In this paper, test pieces Nos. 1 to 3 are intended to be tightly attached to the tanks to simulate the worst case, however the resulting layer density of No. 1 was relatively small (Table 5) due to the technical difficulty involved in the inter-leaved lapping procedure. The average layer density is calculated from the perimeter length for both the cylindrical and rectangular tanks (Fig. 17).

The difference between Nos. 1 and 2 is only the existence of bending corners, in other words, a non-uniform layer density. In the case of a rectangular tank, the perimeter measurement itself is hindered; a soft tape ruler can

12

suppress the layers and renders the layer density slightly larger at the time of measurement in case of small layer density (e.g. the flat area of a rectangular tank). The surface temperature at the corner is measured at six points in case of No. 2, namely 299.5, 299.3, 299.5, 299.1, 299.1 and 299.3K respectively, which are significantly lower than the average temperature (300.1K) in the normal area (far from the corner). The average of these six values at corners is 299.3K, where the local heat flux is predicted at approximately 3.0 W/m², which significantly exceeds the average heat flux (1.36 W/m²) in the whole measurement area. However, the neighboring points located approximately 5mm away from the edge at each side show no significant temperature drop, which indicates that the performance degradation around a corner is localized in a few millimeters on each side. Assuming that the degraded area is 6mm wide (3mm on each side) and the temperature in this width is equal to 299.3K, the total heat leak at four corners can be roughly calculated as 0.022W, while total heat leak is 0.385W. This rough calculation based on surface temperature distribution indicates that the heat leak around the corner exceeds that of the normal area, but is not dominant compared to the total heat leak.

In the case of No. 3, the corner temperature is measured at two points, the results of which are 299.5 and 299.9K, while the average of the normal area is 300.3K. Similarly, the total heat leak at the four corners can be roughly calculated as 0.007W, while the total heat leak is 0.137W. Therefore, the result of No. 3 also elicits the same conclusion.

It was expected before the tests that No. 2 would show a significantly larger total heat leak than No. 1, but the result is actually comparable to the latter, which can be interpreted as showing that more limited degradation at the corner than expected, and may balance out the improvement in performance in the flat area.

Table 5 Averaged layer density of test piece Nos. 1-3

No.	Averaged layer density* [layers/mm]	Shape of Tank
1 (12layers)	2.0	Cylinder
2 (12layers)	4.1	Rectangular
3 (24layers)	3.7	

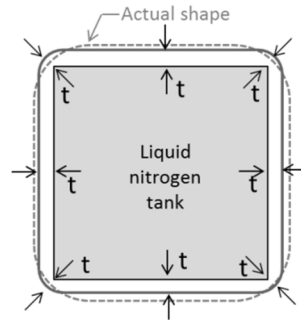*Calculated with the perimeter length of MLI surface

Fig. 17 Averaged thickness in case of a rectangular tank

B. Traditional MLI blanket and MLI-patch technique (Nos. 4-6)

The thermal performances of traditional MLI blankets for spacecraft (Nos. 4 and 5) are significantly worse than the reference MLI with the same number of layers (No. 2); largely due to the existence of stitching[1]-[3]. This is also confirmed with the MLI surface temperature distribution (Figs. 18, 19). The heat leak around the corner (around x=0) can be roughly calculated from the temperature distribution in Fig. 19, which results in approximately 1.0 W per corner (4.0 W/four corners) in the case of No. 4. The total heat leak is 4.5W in the case of No. 4, meaning most of the heat leak results from the stitch and edge effect.

Stimpson & Jaworski [2] proposed an empirical formula of:

$$\Delta Q_{MLI} = 0.0335 + 0.00088 L_{stitch} \qquad (1)$$

where ΔQ_{MLI} denotes the increase in heat leak in watts and L_{stitch} denotes the length of stitches in millimeters. L_{stitch}, is approximately 300mm per corner and the number of stitches is three (one for edge sewing, and two for the hook and loop fastener) in the case of No. 4, which elicits a total heat leak of 3.6W based on their empirical equation. Although there are many differences between their test and ours, the order of heat leak due to stitches can be effectively described using their formula.

The heat flux is reduced into less than one third of by installing an MLI patch for each corner, but still far exceeds the reference (No. 2). It should be noted in Fig. 19 that the temperature drop is mitigated at the corner thanks to the patch, but a cold spot emerges around the edge of the patch-MLI (X=60-70mm). Figure 20 shows the surface temperature distribution of a base-MLI, which indicates the existence of an in-plane heat leak in the films (Fig. 21). The thickness of the aluminum layer deposited on films is approximately 500 angstroms. Considering the temperature gradient seen in Fig. 20, the in-plane heat conduction in the outermost layer (AL is deposited on a single side) of base-MLI and the innermost layer of the patch (AL is deposited on both sides) can

13

be calculated as 0.032W for one edge of the patch, and as 0.256W for eight edges of four patches. This value is considerable compared to the total heat leak of 1.18W. Note that not only these two films but also others will contribute as in-plane heat patches, though the temperature gradient should decline from that of Fig. 20. According to this rough calculation, the difference in heat leaks between Nos. 6 and 2 can be attributed to in-plane heat conduction, or a "thermal short" in other words.
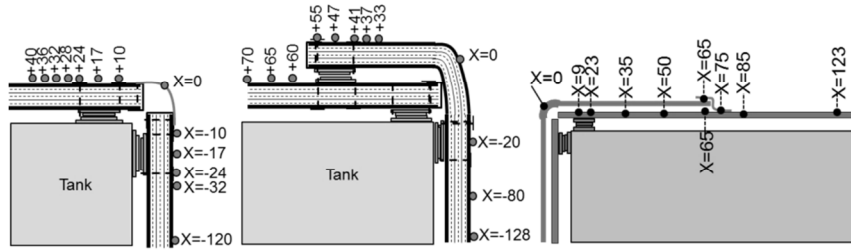

Fig. 18 Thermocouple locations for Nos. 4, 5, and 6.
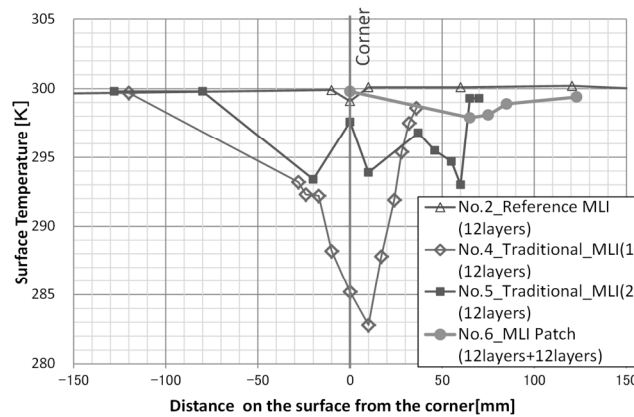

Fig. 19 Surface temperature distribution
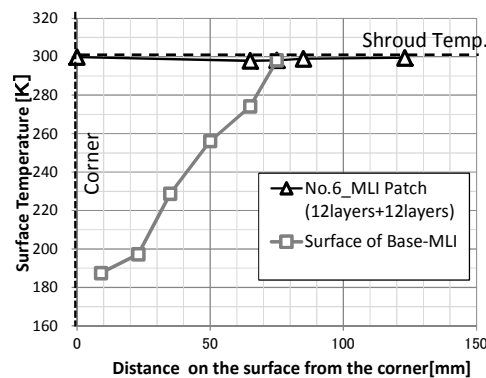
Fig. 20 Temperature distribution on the surface of base-MLI (Nos. 2 and 4)
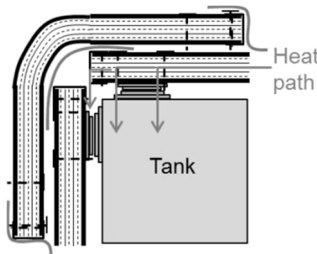
Fig. 21 Heat leak path under the patch

C. **Zero-stitch MLI and Multi-blanket, staggered lapped MLI (Nos. 7-8)**

Zero-stitch MLI and Multi-blanket, staggered lapped MLI show significantly improved thermal performance compared to traditional blanekets (Nos. 4-6) despite having the same fastener interface. The heat fluxes of those exceed the reference of the same number of layers (No. 3), while remaining at the same level even though the workability of blanket production, handling, and blanket connection is much improved and they have a smaller pitch of perforation holes.

14

Figure 22 shows the surface temperature distributions, where no significant temperature drop is seen. The temperatures on the MLI surface just above the tag-pins were measured at four points, the results of which were 300.0, 300.0, 300.1 and 299.5 K for No. 7 at T_{shroud} = 300K, slightly lower than the clean area, although the difference was subject to measurement uncertainty. The mothod used to source the heat leak based on a drop in surface temperature is effective for traditional MLI, but no longer effective for high-performance MLI.

Direct conductive heat leaks through tag-pins (24 pins above the measurement tank) can be calculated as approximately 0.0072W (0.0003 W per pin) in case of T_{shroud} = 300K using the thermal conductivity of PEEK (0.25W/m²K), the dimension of the pin (filament diameter of 0.3mm and 15mm long), and the boundary conditions (T_H=300K and T_C=77K). Since it corresponds to 2.5% of the total heat leak (0.29W) for No. 7, it is not the main reason for the heat loss. Radiative heat loss is likely due to the penetration holes for the tag-pin, but with their limited number and diameter in mind, they seem inconsequential compared to those due to perforations.

Concerning the heat loss due to perforation holes, some literature discusses the relationship between the increase in heat leak, open area, hole diameter and emissivity of the shield surface [5][16]. Using an equation for the small perforation hole proposed by Hinckley[5], the heat loss can be calculated as approximately 30% in case of No. 6 (open area: 0.50%), and 8% in case of No. 3 (open area: 0.12%), compared to the radiative heat loss of the non-perforated shield system. This is considered one reason for the difference in heat leak between Nos. 3 and 6. It should be noted that several other differences exist between those two cases - layer density, number of nets, the existence of a thick PET sheet, number of lapping areas, lapping length, and so on. More experimental data is necessary to discuss the reason for performance degradation of zero-stitch MLI in quantitative terms.

Conversely, multi-blanket, staggered lapped MLI show slightly degraded performance compared to zero-stitch MLI. The number of tag-pins is the same for these two, thus the lapping method is considered the reason for this degradation. The temperature distribution on the surface of each sub-blanket is shown in Fig. 23, while the locations of the thermocouples were already presented in Table 1. As expected, the temperature difference across a sub-blanket is smaller at the edge (e.g. between T/C 2-2 and T/C2-5) than at a clean region (e.g. between T/C 2-3 and T/C 2-7), which indicates the degraded performance at the butt-jointing region of each sub-blanket. Simultaneously, as expected, there are significant temperature differences in-plane (e.g. between T/C2-5 and T/C2-7), which compensate for the poor performance at the butt-jointing region. The conductive heat resistance at the butt-jointed edges of traditional MLI can be roughly calculated as 2.2×10^2 K/W by assuming a surface temperature of 290K at a width of 80mm. In case of 6 layers, the conductance will be half that value (1.1×10^2 K/W). Conversely, in-plane heat conduction is roughly calculated as 1.27×10^4 K/W per a film (AL deposited for both sides) when the lapping length is 90mm, thus, in the case of a 6-layer sub-blanket, peaking at 4.2×10^3K/W by considering that only the first three layers contribute to the conduction in one direction. This in-plane thermal resistance is more than 30 times larger than that of the butt-jointed edges of traditional MLI, namely, the staggered lapping method effectively mitigates the heat leak due to degraded thermal performance at the connection points. In the case of No. 8, the edges of the sub-blanket are not machine-sewn but sewn loosely by hand. An additional test for a test piece comprising four machine-sewn sub-blankets is planned in future.

It is a trade-off problem; how the edges of the sub-blanket are treated, how many sub-blankets the mother blanket is divided into, and the distance between the two neighboring connection points. The design will gradually approach that of the inter-leaved-lapped zero-stitch MLI or "one-by-one method", if the engineers strive ceaselessly to improve performance. However, if a thermal performance requirement is determined and certain limitations imposed, these two MLI designs should be strong options for thermal engineers; they can choose a method which meets the requirement with minimum time and cost.

Fig. 22 Surface temperature distribution
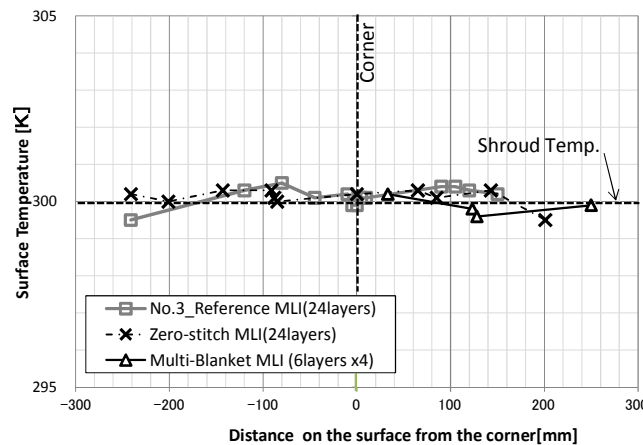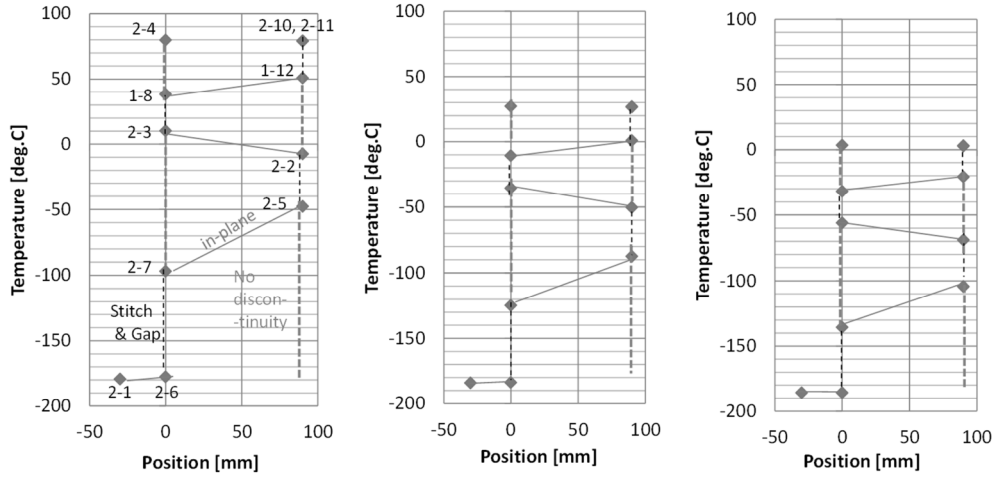
15

Fig. 23 Temperature distribution around a staggered-lapped area

D. Prediction of heat leak at different temperature range

Some experimental equations to predict the temperature dependency of MLI thermal performance are proposed in literature [5][6]. The coefficients of the equation depend on many parameters such as the number of layers, spacer material, material of the vapor-deposited metal layer, pre-treatment method, contact pressure (or layer density), and so on. Although the general form of the equation should resemble those of literature, the coefficients should be evaluated individually per MLI system. Basically, the equation that Cunnington et al.[6] proposed is adopted in this test, while the coefficient of each term is simplified as follows using three free-parameters (A, B and C) since the effect of each parameter is not evaluated in our test:

$$q_{\text{MLI}} = A \times \sigma(T_H^{4.67} - T_C^{4.67}) + (B \times \frac{T_H + T_C}{2} + C) \cdot (T_H - T_c), \qquad (2)$$

where T_H and T_C denotes the temperature of the hot- and cold- side boundaries, σ denotes the Stefan-Boltzmann coefficient and A, B, and C are to be determined with experimental results using the least square method.

Examples of fitting curves for Nos. 7 and 8 are shown in Fig. 24. Although the best fit curve should be identified uniquely per plot combination, many best-fit curves can exist due to the uncertainty of experimental data. However, the worst and best cases can be identified by searching eight patterns involving a combination of maximum and minimum values at each shroud temperature. It is suggested that the predicted heat fluxes of zero-stitch MLI (No. 7) and Multi-blanket, staggered-lapped MLI (No. 8) within the temperature range T_H =120K, T_C=80K are approximately 0.060-0.110W/m² for No. 7 and 0.080-0.130 W/m² for No. 8; both of which unfortunately exceed the target value (0.040W/m² at T_H=120K, T_C=80K).
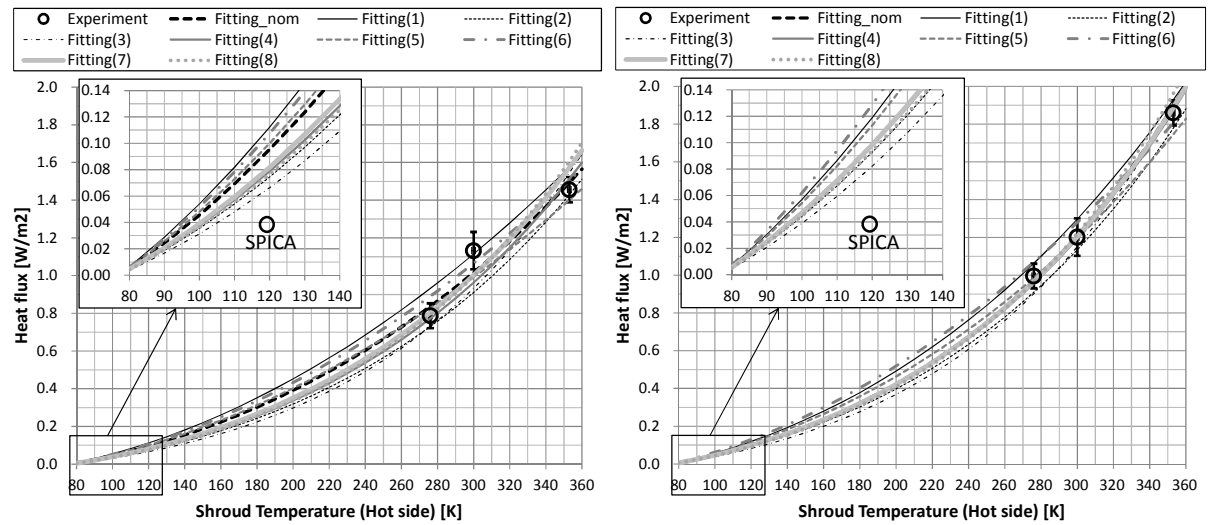

Fig. 24 Heat flux estimation at the temperature level of SPICA
(Left: zero-stitch MLI(No. 7), Right: Multi-blanket, staggered lapped MLI (No. 8))

16

IV. Conclusion

Thermal performance tests using a rectangular boil-off calorimeter were performed to evaluate reference MLIs, traditional MLI blankets, and two new types of MLI using tag-pins; zero-stitch MLI and multi-blanket, staggered lapped MLI.

It is confirmed in this paper that variations in the flow rate of evaporated nitrogen gas from the tanks correlate strongly with the change in atmospheric pressure, and the amplitude of fluctuation can be explained by the shift in the two-phase equilibrium point of nitrogen in the tanks. A correction method that cancels the resulting shift in flow rate is proposed, which is relatively significant when high-performance MLI is tested with a boil-off calorimeter since the variation becomes equivalent to the flow rate value.

Concerning reference MLIs and traditional MLI blankets, abundant literature discusses the effect of various parameters, including layer density and stitch length. New knowledge obtained in this paper is the effect of the bending corner. Even though blankets are intended to be tightly attached to the tank, performance degradation is limited and localized. These precise evaluations are achieved thanks to uniformity in the axial direction in terms of shape and temperature distribution. The results of traditional MLI blankets, the thermal performance of which is in significant decline due to stitches, are also meaningful as a starting point: various techniques to improve performance can be evaluated using the same fastener interface. It should be noted that the thermal performance test for an MLI blanket is usually performed in configurations close to the ideal one.

As far as the author is aware, the tag-pin has never been used to fix MLI blanket layers for flights. Tag-pins made of PEEK, considered compatible for space environment when shielded from direct UV radiation, have been newly developed to achieve the concept of a zero-stitch MLI blanket that can be produced and handled with acceptable effort. Details of the blanket such as the number of pins and perforation hole specification target practical usage, while the validity of the venting design is confirmed in a depressurization test. The thermal performance of zero-stitch MLI is significantly better (ε_{eff} is below 0.0050 at room temperature) than traditional ones (ε_{eff} is approximately 0.030 at room temperature) despite having the same fastener interface. In addition, as a promising option called as a multi-blanket, staggered lapped MLI, which significantly improves the workability of the blanket connection procedure while minimizing performance degradation, is also presented. This is a trade-off problem between thermal performance and practical utility (including weight, cost, venting property, workability, etc.). The result of this paper provides thermal engineers with effective options other than the one-by-one method.

Unfortunately, heat flux at cryogenic temperature, predicted based on literature and test results, does not perfectly match the current SPICA mission requirement, while the requirement itself is not fixed. Some other measures remain to improve blanket performance, for example, by increasing the number of layers, changing the spacer material, controlling the layer density by certain measures, and so on. It should be noted that the test configuration in this paper is close to the worst case in terms of the number of discontinuity, thus the performance is expected to improve when blankets of the same design are installed on a large-sized SPICA radiation shield. The test configuration should be carefully chosen to be worse than the actual configuration, but not excessively severe. In addition, it is quite important to include an atmospheric pressure gauge and level gauge for liquid nitrogen to reduce the uncertainty of the prediction result at the temperature level of SPICA, while testing in cryogenic temperature is more attractive and to be performed in future.

References

[1] J. Doenecke, "Survey and Evaluation of Multilayer Insulation Heat Transfer Measurements," *SAE Technical paper series*, No. 932117, 1993.

[2] L. D. Stimpson and W. Jaworskis, "Effect of Overlaps, Stiches, and Patches on MLI," AIAA paper, No. 72-285, 1972.

[3] E. I. Lin, J. W. Stultz, and R. T. Reeve, "Test-Derived Effective Emittance for Cassini MLI Blankets and Heat Loss Characteristics in the Vicinity of Seams," *AIAA paper*, 95-2015, 1995.

[4] R. B. Hinckley, 'Liquid Propellant Losses During Space Flight,' NASA CR-53336 (1964).

[5] G. R. Cunnington, C. W. Keller and G. A. Bell, 'Thermal Performance of Multilayer Insulation,' NASA CR-72605 (1971).

[6] C. W. Keller, G. R. Cunnington and A. P. Glassford, 'Thermal Performance of Multilayer Insulations,' NASA CR-134477 (1974).

[7] C. Ranzenberger, M. Moser, G. Varewijck, B. Lehmann, H. Ritter, D. Battaglia, and J. Schilke, 'Thermal Performance testing of the BepiColombo high –temperature MLI,' *40th International Conference on Environmental Systems (ICES)* AIAA-2010-6164 (2010).

[8] S. Okazaki, M. Murakami, H. Kawasaki, T. Yabe, H. Sugita, and Y. Kanamori, "Experimental Study of the influence of processing on MLI performance for Space Use," *38th International Conference on Environmental Systems (ICES)* AIAA-2008-01-2067, 2008.

[9] H. Kawasaki, S. Okazaki, H. Sugita and M. Murakami, "Temperature dependence of Thermal Performance in Space using Multilayer Insulation," *52nd International Conference on Environmental Systems (ICES)*, AIAA-2012-3407, 2012.

[10] K. Shinozaki, Y. Sato, K. Sawada, M. Ando, H. Sugita, T. Yamawaki, T. Mizutaki, Keiji Komatsu, T. Nakagawa, H. Murakami, H. Matsuhara, M. Takada, S. Takai, A. Okabayashi, S. Tsunematsu, K. Kanao and K. Narasaki "Thermal study of payload module for the next-generation infrared space telescope SPICA in risk mitigation phase," *Cryogenics* (under review process), 2013.

[11] N. Inai, *Japan Society of Mechanical Engineers*, Vol. 43, No. 365(1977-1), 217, 1977.

[12] R. Hatakenaka, T. Yabe, N. Iwata, H. Ogawa, and M. Saitoh "Inflation and Peel-off Characteristics of MLI Blanket under Depressurization Environment," *42nd International Conference on Environmental Systems (ICES),* AIAA-2012-3406, 2012.

[13] K. Kamiya, M. Furukawa, R. Hatkaenaka, T. Miyakita, H. Murakami, K. Kizu, K. Tsuchiya, Y. Koide, and K. Yoshida, "Electrically Insulated MLI and Thermal Anchor," *Cryogenic Engineering Conference & International Cryogenic Materials Conference (CEC/ICMC 2013)*, 1EPoB5-04, 2013.

[14] S. Jacob, S. Kasthurirengan and R.Karunanithi, "Investigations into thermal performance of multilayer insulation (300-77K) Part 1: Calorimetric studies," *Cryogenics*, **32**, No.12, 1137 (1992).

[15] T. Miyakita, R. Hatakenaka, H. Sugita, M. Saitoh and T. Hirai, "Development of a New Multi-layer Insulation Blanket with Non-Interlayer-Contact Spacer for Space Cryogenic Mission," *Cryogenics* (under review process), 2013.

[16] C. L. Tien, G. R. Cunnington, "Radiation Heat Transfer in Multilayer Insulation having perforated Shields," *AIAA Paper,* 73-718, 1973.